Gas–Solid Interactions During Nonisothermal Heat Treatment of a High-Strength CrMnCN Austenitic Steel Powder: Influence of Atmospheric Conditions and Heating Rate on the Densification Behavior

NIKOLAJ KRASOKHA, SEBASTIAN WEBER, STEPHAN HUTH, KATHRIN ZUMSANDE, and WERNER THEISEN

This work deals with gas–solid interactions between a high-alloyed steel powder and the surrounding atmosphere during continuous heating. It is motivated by the recently developed corrosion-resistant CrMnCN austenitic cast steels. Here, powder metallurgical processing would be desirable to manufacture highly homogeneous parts and/or novel corrosion-resistant metal-matrix composites. However, the successful use of this new production route calls for a comprehensive investigation of interactions between the sintering atmosphere and the metallic powder to prevent undesirable changes to the chemical composition, *e.g.,* degassing of nitrogen or evaporation of manganese. In this study, dilatometric measurements combined with residual gas analysis, high-temperature X-ray diffraction (XRD) measurements, and thermodynamic equilibrium calculations provided detailed information about the influence of different atmospheric conditions on the microstructure, constitution, and densification behavior of a gas-atomized CrMnCN steel powder during continuous heating. Intensive desorption of nitrogen led to the conclusion that a vacuum atmosphere is not suitable for powder metallurgical (PM) processing. Exposure to an N_2-containing atmosphere resulted in the formation of nitrides and lattice expansion. Experimental findings have shown that the N content can be controlled by the nitrogen partial pressure. Furthermore, the reduction of surface oxides because of a carbothermal reaction at elevated temperatures and the resulting enhancement of the powder's densification behavior are discussed in this work.

DOI: 10.1007/s11661-012-1234-1

I. INTRODUCTION

RECENTLY developed high-strength CrMnCN austenitic steels feature excellent mechanical properties and good corrosion resistance.[1–5] In an analogy to Hadfield steels,[6] these materials achieve their strength from their high interstitial content. Being alloyed with carbon and nitrogen, CrMnCN austenites reach yield strengths and true fracture strengths of up to 600 MPa and 2500 MPa, respectively.[4] Furthermore, as a consequence of the combined presence of C + N in the solid solution, the concentration of free electrons is considerably increased, leading to improved short-range atomic ordering, higher solubility of the interstitials in the melt, and an enhanced ductile metallic character of the interatomic bonding.[3,4,7,8] In their experimental investigations of C + N austenites, Berns *et al.*[4] measured elongation values at fracture of up to 74 pct and a specific fracture energy of approximately 700 J/cm^3.

With respect to the constitution, CrMnCN austenites are typically alloyed with 18 – 20 mass-pct Cr and Mn each and with up to 1 mass-pct C + N.[1,2,5] In these steels, chromium is necessary not only for corrosion resistance but also in combination with a high amount of manganese to enhance nitrogen solubility in the melt.[4,5,9] Because of the additional effects of carbon, *i.e.,* stabilization of the face-centered cubic (fcc) phase at higher temperatures and reduction of the δ-ferrite content during solidification, CrMnCN austenites can be produced at atmospheric pressure and do not require cost-intensive pressurized electroslag remelting.[4,5,9]

As the beneficial effects of Cr, N, and C (corrosion resistance and mechanical properties) can be exploited only when these elements are dissolved in the metallic matrix, CrMnCN steels have to be free of precipitates.[5,10,11] However, the potential to form carbides or nitrides during cooling from the solution-annealing temperature increases with increasing C + N content.[4,9] With respect to this limitation, the influence of the amounts of carbon and nitrogen on heat treatability was intensively investigated at the Chair of Materials

NIKOLAJ KRASOKHA, Scientific Assistant, STEPHAN HUTH, Junior Professor, and WERNER THEISEN, Chairholder, are with the Chair of Materials Technology, Ruhr-University Bochum, Universitätsstr. 150, 44801 Bochum, Germany. Contact e-mail: huth@wtech.rub.de SEBASTIAN WEBER, Group Leader, is with the Chair of Materials Technology, Ruhr-University Bochum, and with Helmholtz-Zentrum Berlin für Materialien und Energie GmbH, 14109 Berlin, Germany. KATHRIN ZUMSANDE, Scientific Assistant, is with the Helmholtz-Zentrum Berlin für Materialien und Energie GmbH.

Manuscript submitted August 30, 2011.
Article published online May 30, 2012

Technology of the Ruhr-Universität Bochum (Germany).[12,13] It was found that there is an optimum ratio $(C/N)_{op}$ at which the phase field of homogeneous austenite is extended to the lowest temperature T_{op} (Figure 1). Hence, in addition to the overall interstitial amount, the C/N ratio also has to be considered to ensure optimum performance of the steels.

CrMnCN austenites are currently produced by means of ingot metallurgy. However, the superior properties of the material also make it interesting for powder metallurgical (PM) processing. In comparison with the widely used conventional CrNi austenitic steel AISI 316L,[14–16] significant improvement of mechanical properties can be expected for parts made of high-strength CrMn austenites produced by solid-state sintering. Another application field is observed in the production of corrosion-resistant metal-matrix composites for wear-resistant applications. Qualities such as enhanced strength and work hardening as well as corrosion resistance make the steels highly interesting for the manufacturing of parts exposed to wear and corrosive environments.

Expanding the range of application of these steels by powder metallurgy requires additional investigations to consider new processing conditions and their influence on the material. Sophisticated alloy design of high-strength CrMnCN austenites is responsible for the excellent properties; however, a deep understanding of interactions between the sintering atmosphere and the metallic powder is essential to avoid undesirable changes in the constitution. In their experimental study on the heat treatment of cast CrMnCN steels, Riedner and Berns[12] have found that the nitrogen content in the surface zone is significantly influenced by the nitrogen partial pressure of the applied atmosphere. Consequently, because of the small size and the high specific surface area of atomized powders, special attention has to be paid to gas–solid interactions at elevated temperatures because nitrogen degassing or uptake would result in significant changes to the overall amount of nitrogen.

The aim of this work is to study the influence of atmospheric conditions on microstructural changes, constitution, and densification behavior of gas-atomized CrMnCN steel powder during continuous heating. Investigations of these fundamental processes are expected to offer general indications regarding the suitability of the material for powder metallurgy and the evaluation of different atmospheres with respect to nitrogen uptake or degassing. The effect of the heating rate is also considered. The experimental part of the work is based on dilatometric measurements, residual gas analysis (RGA), and *in situ* high-temperature X-ray diffraction (XRD) experiments. Furthermore, thermodynamic equilibrium calculations are made for different scenarios with respect to the nitrogen partial pressure of the atmosphere. A combinatorial evaluation of the experimental data offers detailed information about the processes taking place inside and on the surface of atomized powder grains and their influence on the densification behavior of the powder fill.

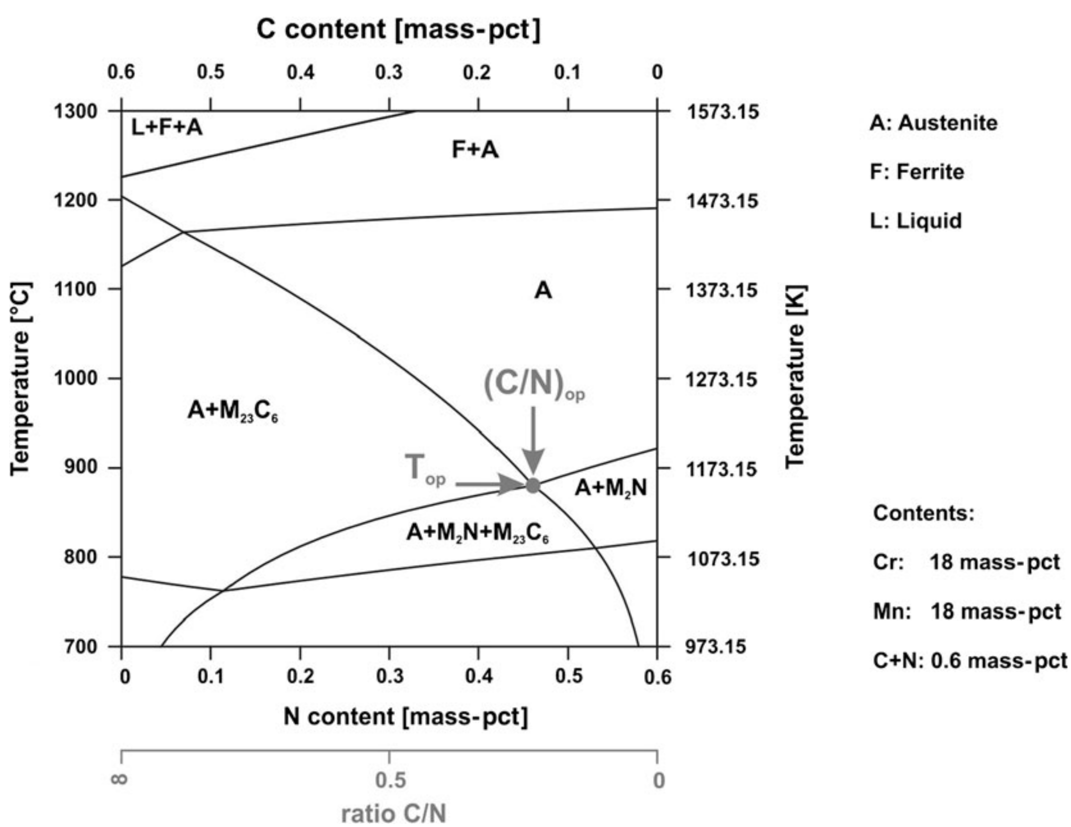

Fig. 1—Phase diagram of a model alloy with 18 mass pct Cr, 18 mass pct Mn, and 0.6 mass pct C + N.

Table I. Chemical Composition of the Investigated CrMnCN Austenitic Steel Powder. Measurements Were Performed on the Prealloyed Ingot before Atomization

	C	N	Cr	Mn	Mo	Ni	Si	Fe
Content (mass pct)	0.36	0.40	18.00	19.20	1.03	0.36	0.38	balanced

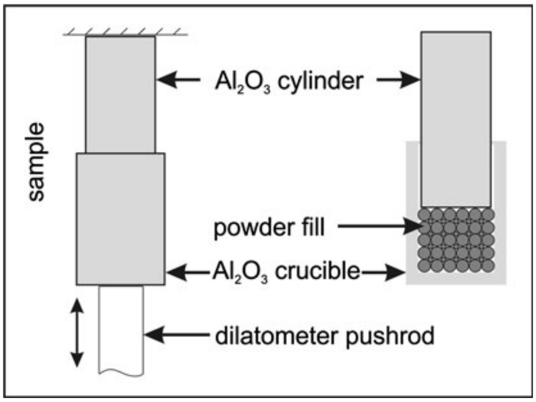

Fig. 2—Schematic drawing of the experimental procedure and sample assembly applied in dilatometric measurements.

II. EXPERIMENTAL

The investigated prealloyed austenitic CrMnCN steel powder was produced by gas atomization in a nitrogen gas stream. The chemical composition is given in Table I. A powder with a particle size smaller than 200 μm was used in this study.

The volumetric behavior of loose powder was investigated by means of dilatometric measurements. Because of the vertical arrangement of the dilatometer (type Linseis L75PT; Linseis, Inc., Robbinsville, NJ), it was not necessary to use precompaction, presintering, or a binder. A schematic drawing of the sample assembly is shown in Figure 2. The samples comprise an Al_2O_3 crucible (inner diameter = 5.1 mm), the powder, and an Al_2O_3 cylinder (outer diameter = 5 mm, height = 20 mm), whereby the crucible is filled with the powder. The cylinder is placed on the top of the filling. Thus, volume changes of the powder can be extracted from the measured data after subtraction of the corresponding temperature-dependent elongation of the alumina components. The contact load between the sample and the measurement system was set to 150 mN. Dilatometric investigations were performed using heating rates ($\dot{T}$) of 5, 10, and 15 K/min and three different atmospheres: vacuum (approximately 1 Pa), 0.03 MPa N_2, and 0.1 MPa N_2.

RGA was performed with an e-Vision analyzer (MKS Instruments, Rochester, NY) equipped with tungsten filaments and a Faraday detector. The device was attached to the dilatometer furnace (used to heat the samples) and operated with an electron energy of 70 eV and an emission current of 1 mA at a maximum pressure of 1×10^{-2} Pa.

A phase analysis was performed with an X-ray diffractometer (Bruker AXS, Inc., Madison, WI) equipped with a cobalt X-ray source and a Ge monochromator. The distance between the sample and the detector was 250 mm. Measurements at room temperature (293.15 K [20 °C]) were performed with a counting time of 30 minutes. For high-temperature experiments, loose powder fractions were heated to 973.15 K (700 °C), 1173.15 K (900 °C), and 1273.15 K (1000 °C) followed by an acquisition time of 5 minutes.

Thermodynamic equilibrium calculations were carried out with Thermo-Calc software version S (Thermo-Calc, Canonsburg, PA) and the thermodynamic database TCS Steel and Fe-alloys Database, v6 (TCFE 6.2; Thermo-Calc). In calculations for a constant chemical composition and Scheil simulations, data for the following phases were retrieved: LIQUID, BCC_A2, FCC_A1, HCP_A3, CEMENTITE, M23C6, M7C3, and M6C. To consider different atmospheric conditions (nitrogen partial pressures), the GAS phase was also included in calculations and its amount was set to zero, the condition for the nitrogen content was deleted, and the pressure of the system was set to the corresponding N_2 partial pressure.

III. RESULTS

A. *As-Atomized Austenitic Steel*

Characterization of the austenitic steel in the as-atomized state was carried out by means of microstructural investigations (scanning electron microscopy [SEM]) and X-ray analysis. Furthermore, Scheil calculations were performed to consider possible phase formations during solidification of the powder grains.

A representative micrograph of the powder is shown in Figure 3. As a result of the last polishing step oxide polishing suspension (OPS), the crystallographic grains are clearly visible. Despite the relatively high chromium and carbon contents of 18 mass pct and 0.36 mass pct, respectively, the micrographs show no grain boundaries decorated by eutectic carbides or secondary precipitations. More information about the microstructure in as-atomized state was extracted from the X-ray measurements at room temperature. In addition to the austenitic reflections, ferrite can also be identified in the diffractogram illustrated in Figure 4. This observation is consistent with the Scheil-Gulliver solidification simulation presented in Figure 5 in which ferrite is calculated to be the first solid phase in the system. In contrast, precipitation of $M_{23}C_6$ seems to be overestimated by the solidification simulation because no carbides are observed in the experimental results (Figures 3 and 4).

B. *Dilatometric Measurements*

Influence of atmospheric conditions and heating rate on the temperature-dependent volumetric behavior of

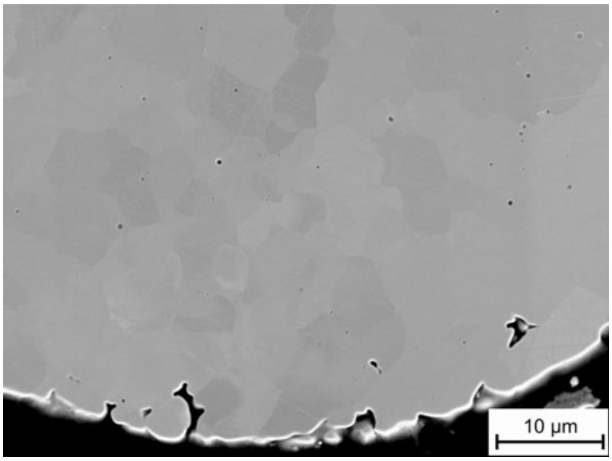

Fig. 3—SEM micrograph of CrMnCN powder in the as-atomized state (secondary electron contrast).

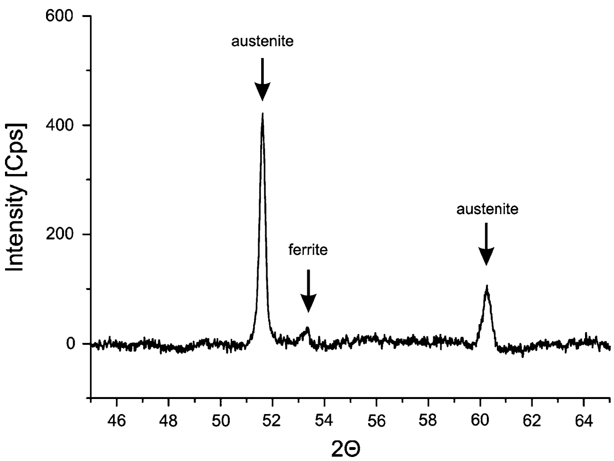

Fig. 4—XRD measurement results and phase identification for CrMnCN powder in the as-atomized state.

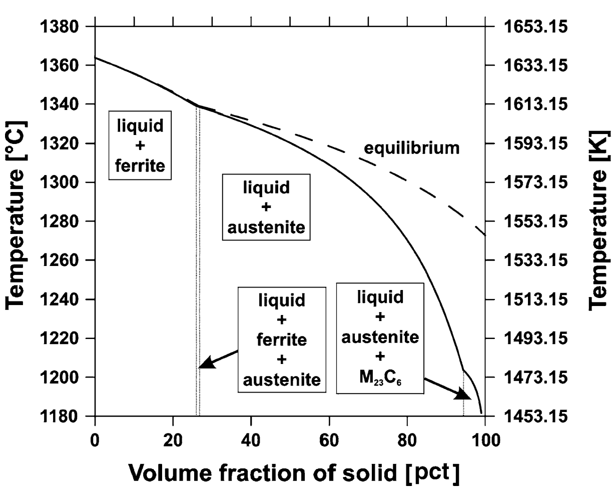

Fig. 5—Scheil simulation of the phase development during solidification of the CrMnCN powder.

the powder was investigated by dilatometric measurements. The results are presented in Figures 6 through 8 as elongation *vs* temperature curves. The curves in

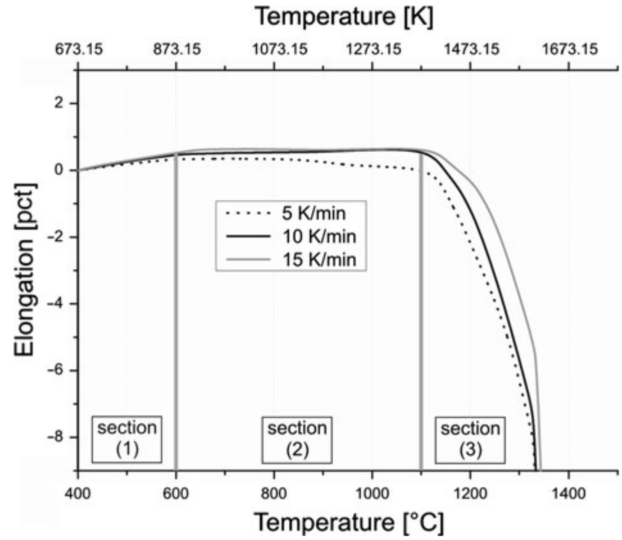

Fig. 6—Results of dilatometric measurements of loose CrMnCN powder in a vacuum atmosphere expressed by elongation/temperature curves.

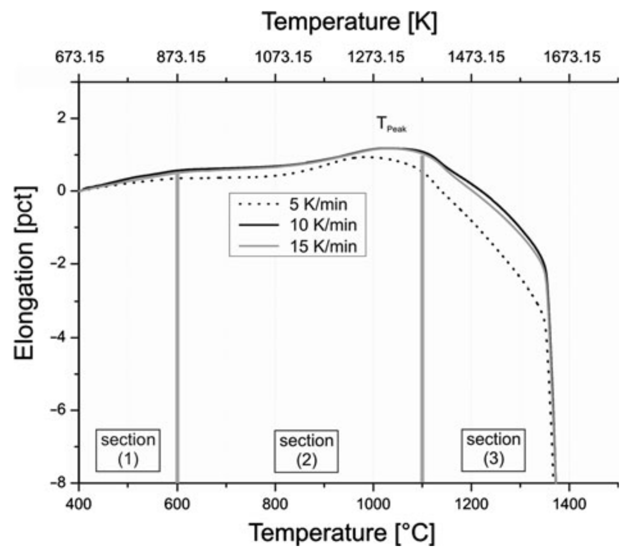

Fig. 7—Results of dilatometric measurements of loose CrMnCN powder in a 0.03 MPa N_2 atmosphere expressed by elongation/temperature curves.

Figure 9 represent measurements performed with the same heating rate of 10 K/min. They show that the atmosphere influences the volumetric behavior.

Starting with the experimental results obtained by measurements in a vacuum atmosphere (Figure 6) at different heating rates (5, 10, and 15 K/min), a general partition of the curves into three sections can be made: (1) almost linear elongation at $T <$ 873.15 K (600 °C), (2) plateau-like progression between 873.15 K (600 °C) and 1373.15 K (1100 °C), and (3) intensive shrinkage at $T >$ 1373.15 K (1100 °C). An influence of the heating rate on the volumetric behavior of the metallic powder can already be observed in section (2) in Figure 6. Whereas the 10 K/min and 15 K/min curves are nearly congruent and exhibit one slight volume increase at

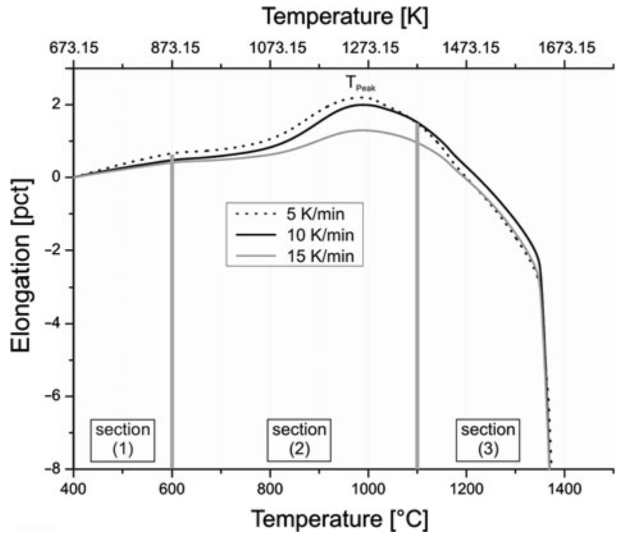

Fig. 8—Results of dilatometric measurements of loose CrMnCN powder in a 0.1 MPa N_2 atmosphere expressed by elongation/temperature curves.

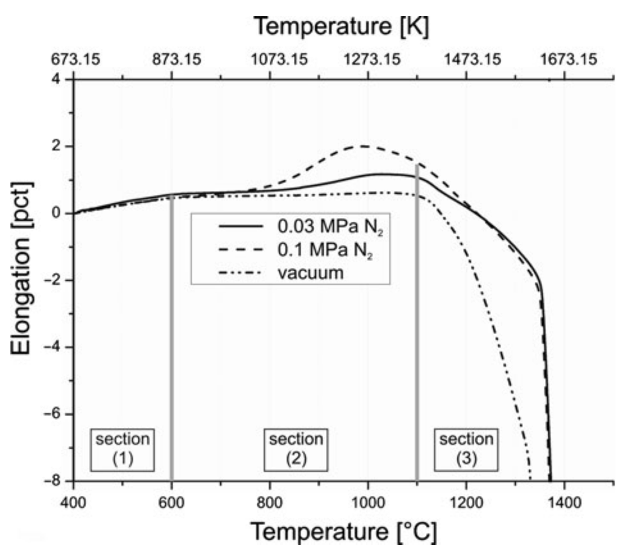

Fig. 9—Comparison of dilatometric measurements of loose CrMnCN powder in a vacuum, 0.03 MPa N_2, and 0.1 MPa N_2 atmospheres. These experiments were performed with a heating rate of 10 K/min.

temperature values around 1173.15 K (900 °C), the 5 K/min curve generally proceeds at lower elongation values and even shows a volume decrease at $T > 1123.15$ K (850 °C). At the beginning of section (3) of Figure 6 all three curve progressions change from plateau-like to negatively sloped, whereby the alteration is influenced by the heating rate: The higher the heating rate, the higher is the alteration temperature. Independent of the applied heating rate, the end of section (3) of Figure 6 is marked by a strong volume decrease at approximately 1603.15 K (1330 °C) in all curves.

Graphs corresponding to measurements in nitrogen atmosphere are presented in Figures 7 and 8. Under both atmospheric conditions (0.03 and 0.1 MPa N_2) up to a temperature range of approximately 1023.15 K to 1073.15 K (750 °C to 800 °C), the densification behavior of the powder is similar to that observed in vacuum experiments (Figure 6). Applying the same partitioning of the graphs as in Figure 6 (with respect to the temperature scale) to the results of the "nitrogen" measurements, one can clearly observe a volume peak in section (2) of Figure 6 between 1073.15 K and 1423.15 K (800 °C and 1150 °C) (Figures 7 and 8). In section (3) of Figure 6, all curves show similar behavior and indicate compaction of the austenitic powder with the densification rate increasing with rising temperature. At 1623.15 K (1350 °C), the progressions of all curves change significantly by featuring one intensive volume decrease.

With respect to the heating rate, no deviations of the curves can be observed on comparing results at 10 and 15 K/min in a nitrogen atmosphere of 0.03 MPa (Figure 7). In contrast, the progression of the 5 K/min curve differs from the last two: The volume peak in section (2) of Figure 6 is generally shifted to lower temperatures and indicates a higher volume increase if the difference between elongation values at the peak onset and the maximum is considered. In case of 0.1 MPa nitrogen experiments (Figure 8), the 5 K/min and 10 K/min curves appear alike, whereas the 15 K/min curve differs. The position of the peak at the temperature scale is similar, but the elongation value of the peak maximum is significantly lower if a heating rate of 15 K/min is used.

C. *Thermodynamic Calculations*

Within the scope of this work, thermodynamic calculations were also performed for the austenitic steel. The results are shown in Figure 10 as phase fraction *vs* temperature diagrams. The calculations were carried out for four different scenarios. In Figure 10(a), the nitrogen content of the steel was kept constant over the entire temperature range. In Figures 10(b) through (d), phase amounts are calculated for the equilibrium nitrogen content of the steel at defined nitrogen partial pressures of 1 Pa (vacuum), 0.03 MPa, and 0.1 MPa, respectively.

When the nitrogen content was kept constant (Figure 10(a)), the steel features two kinds of precipitates: chromium-rich $M_{23}C_6$ and M_2X, where X represents the species N and C, whereby nitrogen is the major element in the composition. At 1188.15 K and 1333.15 K (915 °C and 1060 °C), the M_2X and $M_{23}C_6$ precipitates are dissolved and the steel stays fully austenitic up to a temperature of 1548.15 K (1275 °C), at which formation of the liquid phase and ferrite takes place. T_{Liq} is reached in equilibrium at 1638.15 K (1365 °C).

In the equilibrium calculations for the vacuum scenario (nitrogen partial pressure of 1 Pa) presented in Figure 10(b), the dissolution temperatures of the precipitates are shifted compared with Figure 10(a): The M_2X-phase is not present above 1073.15 K (800 °C), and $M_{23}C_6$ carbides remain stable up to 1418.15 K (1145 °C). Furthermore, ferrite appears between 1073.15 K and 1673.15 K (800 °C and 1400 °C). T_{Sol} and T_{Liq} can be detected at 1508.15 K and 1673.15 K (1235 °C and 1400 °C), respectively.

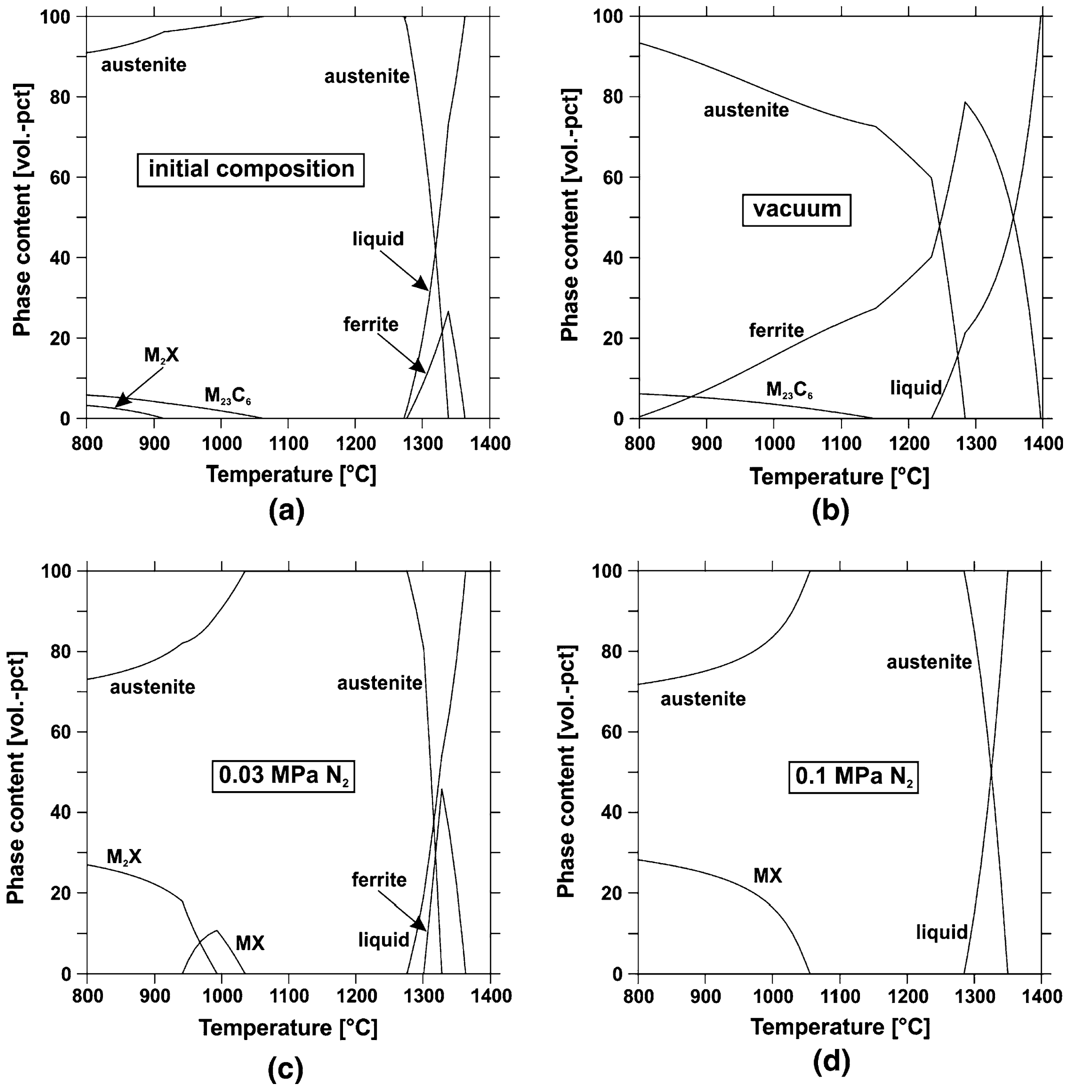

Fig. 10—Thermodynamic equilibrium calculations of the phase contents as a function of the temperature for a CrMnCN steel powder: (*a*) chemical composition is fixed to the initial value, (*b*) nitrogen partial pressure is set to 1 Pa, (*c*) nitrogen partial pressure is set to 0.03 MPa, (*d*) nitrogen partial pressure is set to 0.1 MPa.

Figure 10(c) presents the calculated phase content as a function of the temperature for nitrogen partial pressure of 0.03 MPa. Under this condition, two different types of precipitates are thermodynamically stable at $T > 1073.15$ K (800 °C). The MX type (chromium-rich phase containing nitrogen and a small amount of carbon) features a dissolution temperature of 1268.15 K (995 °C), whereas M_2X appears in the temperature range between 1213.15 K and 1308.15 K (940 °C and 1035 °C). T_{Sol} can be identified at 1553.15 K (1280 °C) and T_{Liq} at 1638.15 K (1365 °C). Within the melting range, a ferritic phase is also present (1573.15 K [1300 °C] to 1638.15 K [1365 °C]). In contrast, according to calculations for a nitrogen partial pressure of 0.1 MPa (Figure 10(d)), only MX precipitates can be identified below 1333.15 K (1060 °C). Furthermore, formation of the ferrite at higher temperatures is completely prevented and the liquid phase ranges from 1558.15 K to 1623.15 K (1285 °C to 1350 °C).

D. *Residual Gas Analysis*

The results of the residual gas analysis performed on the austenitic PM steel are illustrated in Figure 11. Because of the high nitrogen content of the investigated material, two major gas–solid interaction reactions are expected at elevated temperatures: In addition, to carbothermal reduction of the surface oxides, nitrogen exchange between atomized powder grains and atmosphere can also occur. As both molecular nitrogen N_2 and carbon monoxide CO have masses of 28, mass 14 (indicator for nitrogen) and mass 12 (indicator for carbon monoxide) are also shown in Figure 11 to distinguish the two reactions.

Up to 1173.15 K (900 °C), the mass 28 curve progresses nearly horizontally and gives no hint of reactions at lower temperatures. However, a detailed look at mass 12 shows an increase in the signal at approximately 1093.15 K (820 °C), which indicates the onset of the carbothermal reaction. The curve reaches its

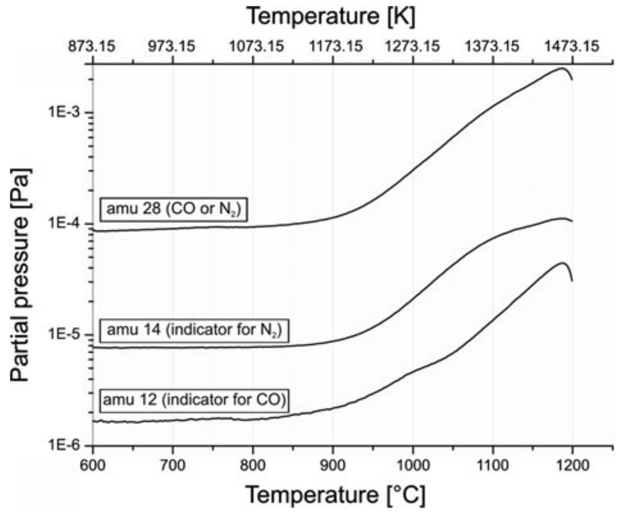

Fig. 11—Results of the residual gas analysis during continuous heating (10 K/min) of the CrMnCN powder.

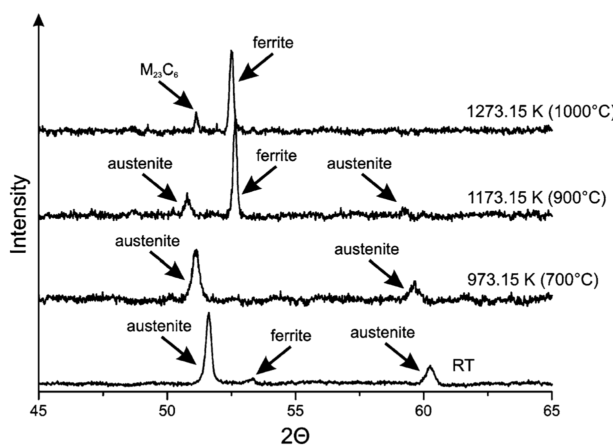

Fig. 12—High-temperature XRD measurement results and phase identification for the CrMnCN powder at room temperature, 973.15 K, 1173.15 K, and 1273.15 K (700 °C, 900 °C,and 1000 °C).

maximum at 1453.15 K (1180 °C). The onset of nitrogen degassing is detected at slightly higher temperatures after the carbothermal reaction starts. The signal of mass 14 leaves its constant level and starts to increase progressively at 1173.15 K (900 °C). After exceeding 1373.15 K (1100 °C), the slope of the curve decreases and the degassing rate becomes more moderate.

E. *High-Temperature XRD*

Figure 12 shows the X-ray diffraction results of the austenitic powder at the chosen temperatures. In contrast to measurements at room temperature (at which a low amount of ferrite is present), only the austenitic phase can be identified at 973.15 K (700 °C). The measured intensities of the sample heated to 1173.15 K (900 °C) are dominated by peaks associated with ferrite, but they still reveal austenite. At the highest temperature of 1273.15 K (1000 °C), only ferrite and $M_{23}C_6$ can be determined.

IV. DISCUSSION

First of all, it should be pointed out that the information extracted from the dilatometric measurements gives a summarized description of the volumetric behavior and arises from different effects, *i.e.*, thermal expansion, reordering of the powder grains, phase transformations, sintering processes, and changes in the chemical composition. These can occur simultaneously and in various combinations.

Based on the results illustrated in Figure 9, there is clear evidence for identical behavior of the steel powder independently of the surrounding atmosphere up to a temperature of 1023.15 K (750 °C). This observation is in agreement with Fast's[17] results. In experiments on pure iron exposed to an N_2 atmosphere, no significant nitrogen absorption was observed below 1173.15 K (900 °C). Furthermore, from industrial applications, it is known that nitrogen is a protective atmosphere up to 1073.15 K (800 °C) because no significant dissociation of the N_2 molecules takes place at lower temperatures.[18,19] As the passivity of N_2 is also obvious in case of the investigated austenitic steel, the behavior of the material between 673.15 K and 1023.15 K (400 °C and 750 °C) will be discussed independently from the applied atmospheric conditions.

The nearly linear elongation of the samples at lower temperatures (<873.15 K [600 °C]) can be interpreted as a thermal expansion of the metallic powder. However, the plateau-like behavior of the curves above 873.15 K (600 °C) indicates additional processes that occur in the temperature range and compensate thermal expansion. Because a low ferrite content was already indicated in the as-atomized state, it is plausible to assume that the transformation of δ-ferrite to the thermodynamically stable and more dense austenite occurs around 873.15 K (600 °C), which compensates thermal expansion of the powder. The disappearance of ferrite after heating to 973.15 K (700 °C) was also confirmed in high-temperature XRD measurements (Figure 12).

Above 1023.15 K (750 °C), the volumetric behavior of the powder is clearly influenced by the applied atmosphere (Figure 9). Starting with vacuum experiments (Figure 6), in case of 10 K/min and 15 K/min curves, the samples exhibit a slight volume increase between 1173.15 K and 1373.15 K (900 °C and 1100 °C). This is caused by the formation of ferrite as a result of the loss of nitrogen and destabilization of the austenitic phase when the powder is exposed to a vacuum. Residual gas analysis has revealed degassing of the nitrogen above 1173.15 K (900 °C) because the mass 14 signal increases in this temperature range. Stabilization of the ferrite is concluded from thermodynamic calculations and high-temperature XRD measurements. In contrast to the calculated phase content diagram for a constant chemical composition (Figure 10(a)), formation of the body-centered cubic phase is shifted to significantly lower temperatures (1073.15 K [800 °C]) when the nitrogen partial pressure of 1 Pa is assumed (Figure 10(b)). An experimental observation of ferrite formation is presented in Figure 12. The intensities of the sample at 1173.15 K (900 °C) are dominated by ferrite peaks, whereas only a low content of austenite remains. The loss of nitrogen and formation of ferrite were also observed by Riedner and Berns[5,12] for a similar steel produced by casting when heat treatment in a vacuum was applied.

At temperatures over 1373.15 K (1100 °C), the metallic powder responds by a volume decrease, which proceeds continuously up to 1603.15 K (1330 °C) (Figure 6). This observation leads to the conclusion that the sintering ability of the powder is significantly improved in this temperature range. A detailed look at the experimental outcome of the RGA measurements (Figure 11) clearly reveals that the highest CO concentration in the atmosphere (indicated by mass 12) is reached at 1453.15 K (1180 °C). Because the signal for mass 12 arises from the reduction of the surface oxides by a carbothermal reaction, it is plausible to assume that the diffusion-retarding layer of the oxides is partially removed and the metallic surface can participate in the sintering process. Taking account of investigations dealing with reduction kinetics of surface oxides, partial elimination of less stable Fe and Cr oxides is likely.[20–22] However, the thermodynamically highly stable Cr-Mn spinels are not believed to be reduced.[21] In addition to the improved surface state as a result of the carbothermal reaction, formation of the liquid phase can also occur above 1508.15 K (1235 °C) (Figure 10(b)). Partial melting of the powder particles leads to viscous flow and, thus, to a beneficial effect on the densification behavior.[24,25]

The end of section (3) in Figure 6 is marked by a very rapid volume decrease of the samples at 1603.15 K (1330 °C). Taking into account the results of thermodynamic calculations, this temperature is not believed to be T_{Sol}. Furthermore, from literature dealing with supersolidus liquid-phase sintering, it is well known that the typical rapid densification occurs not at the solidus temperature but when a certain amount of the liquid phase is present.[25] According to calculations presented in Figure 10(b), the liquid phase content at 1603.15 K (1330 °C) is approximately 35 vol pct, which is in good agreement with values known from corresponding publications.[23,25] The influence of the nitrogen partial pressure on T_{Sol} has to be investigated systematically in future work by means of differential thermal analysis.

In contrast to vacuum experiments, application of a nitrogen atmosphere already leads to significant deviations at 1073.15 K (800 °C) (Figure 9). The plateau-like behavior changes to a peak onset, and the curves reach their elongation maximum at 1273.15 K to 1323.15 K (1000 °C to 1050 °C). This effect is connected to an uptake of nitrogen from the atmosphere and is explained by two simultaneous processes: first, an increase in the lattice parameters caused by an increasing nitrogen content in the solid solution[26,27] and second, the precipitation of M_2N and MN nitrides.[12,27,28] The latter leads to a volume expansion because both nitrides have a lower density than the austenitic matrix of the steel.[29]

More information about the microstructural processes at $T < T_{Peak}$ can be extracted from thermodynamic equilibrium calculations. However, prior to the interpretation of experimental data, limitations of the CALPHAD method have to be discussed. Both conditions—thermodynamic stability of N_2 molecules and absorption rate of nitrogen at the metallic surface—are not implemented in the calculations. Furthermore, the diffusion of absorbed nitrogen from the surface into the material is not considered because of the equilibrium approach of the CALPHAD method. As a consequence, the discrepancy between the calculated and the actual N content of the steel during continuous heating increases with decreasing temperature. Although the nitrogen content of the material (Figure 13) as well as the resulting amount of nitrides (Figures 10(a) and (b)) are overrated in the temperature range, the sequence of the processes, *i.e.,* expansion of the metallic matrix and precipitation of the nitrides, can be analyzed based on calculations presented in Figure 13. When a 0.1 MPa N_2 atmosphere is applied, the nitrogen concentration in the matrix remains nearly constant between 973.15 K and 1173.15 K (700 °C and 900 °C). For this reason, no significant changes in the lattice parameters are expected in the temperature range, and the absorbed nitrogen is assumed to participate primarily in the formation of nitrides. Above 1173.15 K (900 °C), the solubility of N in the metallic matrix increases significantly (up to 1.75 mass pct at 1323.15 K [1050 °C]), leading to an expansion of the lattice and a dissolution of the nitrides.

When the steel is heated above the peak temperature (T_{Peak}), a decrease of the volume is observed (Figures 7 and 8). Taking into consideration the decreasing N content of the material with rising temperature (Figure 13), this effect can be explained by desorption of nitrogen, leading to the dissolution of nitrides and a decrease in the interstitially soluted N content. Because the dilatometric curves were produced by continuous heating of the samples, the suitability of thermodynamic equilibrium calculations was proved by additional

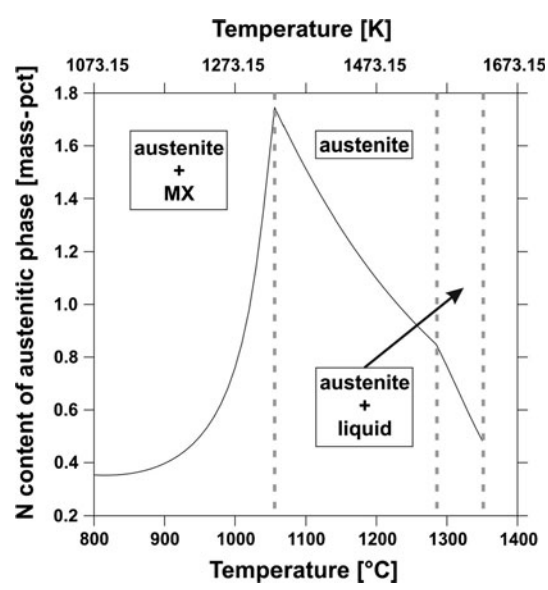

Fig. 13—Calculated nitrogen content of the fcc phase as a function of the temperature at a nitrogen partial pressure of 0.1 MPa.

Table II. Comparison of Measured and Calculated Nitrogen Contents at Different Temperatures and a Nitrogen Partial Pressure of 0.03 MPa

	Mass pct Nitrogen in the Steel at		
	1028.15 K (755 °C)	1333.15 K (1060 °C)	1508.15 K (1235 °C)
Measured	0.42	0.86	0.72
Calculated	4.99	1.14	0.61

quenching experiments: The samples were heated to 1028.15 K (755 °C), 1333.15 K (1060 °C), and 1508.15 K (1235 °C), respectively, using a heating rate of 10 K/min in a 0.03 MPa N_2 atmosphere and then quenched. The nitrogen contents were measured by means of combustion analysis and are listed in Table II along with the calculated values. As mentioned at lower temperatures (1028.15 K [755 °C]), the N content is overestimated in the calculations; however, above 1333.15 K (1060 °C) good agreement is found between measured and calculated results. Based on these results, it can be concluded that during continuous heating, the steel powder reaches its maximum nitrogen content at T_{Peak}.

In this work, the well-known dependence of the nitrogen content in the steel (which correlates with the height of the peak) and the nitrogen partial pressure[9,17,30–34] was also observed in dilatometric curves (Figure 8). Comparing the results obtained at 0.03 MPa and 0.1 MPa N_2 atmospheres provides clear evidence for an increase in the peak height with increased nitrogen partial pressure.

Furthermore, the peak temperature (T_{Peak}) provides information about limiting processes with respect to nitrogen exchange between the atmosphere and the metallic powder. Rates for both events—absorption and desorption of nitrogen—are determined not by the diffusion of nitrogen in metal but by surface reactions[17,35,36]

$$\mathrm{N_2(gas)} \rightarrow \mathrm{N_{2\,ads}(surface)} \rightarrow \mathrm{2N_{ads}(surface)} \rightarrow \mathrm{2N_{diss}(metal)} \quad [1]$$

and

$$\mathrm{2N_{diss}(metal)} \rightarrow \mathrm{2N_{ads}(surface)} \rightarrow \mathrm{N_{2\,ads}(surface)} \rightarrow \mathrm{N_2(gas)} \quad [2]$$

Reactions [1] and [2] control nitrogen exchange at temperatures below and above the peak temperature, respectively. However, at temperatures above T_{Peak}, the good agreement of nitrogen contents measured in quenching experiments with equilibrium calculations (Table II) provides evidence for the reaction rates (reaction [2]) being high enough to ensure a near-equilibrium amount of N in the austenitic steel powder, even during continuous heating with 10 K/min.

Above 1423.15 K (1150 °C), contraction of the samples (Figures 7 and 8) arises from several effects: dilation of the lattice as a result of nitrogen desorption, solid-state sintering, and subsequent formation of the liquid phase. Clear separation and impact evaluation of single events cannot be performed based on dilatometric curves in the temperature range because the processes take place simultaneously and affect volumetric behavior of the samples alike—leading to a volume decrease. Nevertheless, in analogy to vacuum experiments (Figure 6) at 1623.15 K (1350 °C), a certain amount of liquid phase is present and results in a rapid decrease in volume.

In this work, the heating rate was not found to have a significant effect on the compaction behavior. In case of vacuum experiments (Figure 6) the volume decrease between 1173.15 K (900 °C) and 1373.15 K (1100 °C) in the 5 K/min curve in contrast to the volume increase observed for heating rates of 10 and 15 K/min can be explained by more time being available for sintering processes (overcompensation of the volume increase when ferrite forms). The likewise time-dependent nitrogen absorption [Reaction (1)] leads to a shift of TPeak to lower values with decreasing heating rate when nitrogen atmosphere is applied (Figures 7 and 8). However, at higher temperatures, the role of the heating rate diminishes and the volumetric behavior is clearly dominated by temperature. Hence, subsequent progressions of corresponding curves appear alike.

V. SUMMARY AND CONCLUSIONS

The volumetric behavior of a gas-atomized CrMnCN steel powder was investigated with respect to the influence of atmospheric conditions and the heating rate. By combining experimental results obtained from dilatometric measurements with residual gas analysis, high-temperature *in situ* XRD measurements, and thermodynamic equilibrium calculations, it was possible to extract detailed information about surface reactions, phase development, and sintering behavior of the investigated metallic powder during continuous heating.

It was found that below 1023.15 K (750 °C), the material behaves independently of the applied atmosphere because there is no significant absorption or desorption of nitrogen. The volume changes are dominated by thermal expansion and the transformation of δ-ferrite to the austenitic phase. Above 1073.15 K (800 °C), the atmosphere had a significant impact on the nitrogen content of the steel powder, the oxidation state of the particles, and the resulting sintering behavior. In a vacuum atmosphere, degassing of nitrogen takes place above 1173.15 K (900°C), leading to destabilization of the fcc structure and formation of ferrite. Furthermore, a reduction of surface oxides because of a carbothermal reaction was detected by means of residual gas analysis, whereby the highest CO concentration in the atmosphere was measured at 1453.15 K (1180 °C). Consequently, the densification rate of loose powder already improves significantly above 1373.15 K (1100 °C) and is additionally enhanced by the subsequent formation of the liquid phase. However, intensive desorption of nitrogen already during continuous heating leads to the conclusion that a vacuum atmosphere is not suitable for sintering CrMnCN steel powders.

In experiments using an N_2 atmosphere (0.03 and 0.1 MPa), considerable nitrogen absorption by CrMnCN steel powder was observed above 1023.15 K (750 °C). The nitrogen uptake between 1023.15 K and 1323.15 K (750 °C and 1050 °C) resulted in a volume increase as a result of the expansion of the lattice and precipitation of nitrides. Desorption of N_2 took place at temperatures above 1323.15 K (1050 °C). Based on a good agreement between measured and calculated equilibrium N contents at $T > T_{\mathrm{Peak}}$, it was concluded that even during continuous heating with $\dot{T} = 10$ K/min, the reaction rate corresponding to reaction [2] is high enough to allow the amount of N in the steel powder to be close to the equilibrium value. This finding opens new perspectives for PM processing of CrMnCN steels. There is obviously no need to produce powders prealloyed with nitrogen because the final N content of the parts can be precisely adjusted by using an appropriate nitrogen partial pressure for the sintering atmosphere. Manufacturing of N-free powders not only would simplify alloying of the melt before atomization but also would be advantageous for the preparation of green compacts on account of their improved compressibility.

With respect to the heating rate at temperatures relevant for the sintering process, it was observed that the influence of $\dot{T}$ diminishes and the densification behavior of the metallic powder is clearly dominated by parameters such as the nitrogen partial pressure and the temperature.

ACKNOWLEDGMENT

The authors gratefully acknowledge financial support from the German Research Foundation (DFG) within the projects TH 531/8-1 and WE 4436/3-1. We thank the Max-Planck-Institut für Eisenforschung GmbH for supplying high-temperature XRD measurement data.

REFERENCES

1. B.D. Shanina, V.G. Gavriljuk, H. Berns, and F. Schmalt: *Steel Res.*, 2002, vol. 73 (3), pp. 105–13.
2. V.G. Gavriljuk, A.I. Tyshchenko, O.N. Razumov, Y.N. Petrov, B.D. Shanina, and H. Berns: *Mater. Sci. Eng. A*, 2006, vol. 420, pp. 47–54.
3. V.G. Gavriljuk, B.D. Shanina, and H. Berns: *Mater. Sci. Eng. A*, 2008, vols. 481–482, pp. 707–12.
4. H. Berns, V.G. Gavriljuk, S. Riedner, and A.I. Tyshchenko: *Steel Res.*, 2007, vol. 78 (9), pp. 714–19.
5. S. Riedner: Ph.D. Dissertation, Ruhr-Universität Bochum, Bochum, Germany, 2010.
6. R.A. Hadfield: *Metallurgy and its Influence on Modern Progress*, Chapman and Hall, London, U.K., 1925, pp. 91–101.
7. V.G. Gavriljuk, B.D. Shanina, and H. Berns: *Acta Mater.*, 2000, vol. 48, pp. 3879–93.
8. B.D. Shanina, V.G. Gavriljuk, and H. Berns: *Steel Res.*, 2007, vol. 78 (9), pp. 724–28.
9. V.G. Gavriljuk and H. Berns: *High Nitrogen Steels*, Springer-Verlag, Berlin, Germany, 1999, pp. 100–02, 113–15, 130–34, 203–05, 263–71.
10. H. Berns, V.G. Gavriljuk, N. Nabiran, Y.N. Petrov, S. Riedner, and L.N. Trophimova: *Steel Res.*, 2010, vol. 81 (4), pp. 299–307.
11. H. Berns, B. Hussong, S. Riedner, and F. Wischnowski: *Steel Res*, 2010, vol. 3 (81), pp. 245–51.
12. S. Riedner and H. Berns: *J. Heat Treat. Mater*, 2008, vol. 63 (2), pp. 84–94.
13. H. Berns and S Riedner: *J. Heat Treat. Mater*, 2008, vol. 63 (6), pp. 337–41.
14. S.S. Panda, V. Singh, A. Upadhyaya, and D. Agrawal: *Scripta Mater.*, 2006, vol. 54, pp. 2179–83.
15. C. Padmavathi, A. Upadhyaya, and D. Agrawal: *Scripta Mater.*, 2007, vol. 57, pp. 651–54.
16. P. Samal, J. Pannell, U. Engström, and O. Mars: *World PM2010 Proceedings*, Fortezza da Basso Centre, Florence, Italy, 2010, vol. 3, pp. 201–08.
17. J.D. Fast: *Interaction of Metals and Gases,* vol. 1*, Thermodynamics and Phase Relations*, Academic Press, New York, NY, 1965, pp. 122–23, 148–52.
18. H. Berns: *Industrial Heating*, 2003, vol. 70 (5), pp. 47–50.
19. H. Berns, B. Edenhofer, and R. Zaugg: *Trans. Mater. Heat Treat*, 2004, vol. 25 (5), pp. 354–59.
20. H. Borgström and L. Nyborg: *Powder Metall*, 2006, vol. 49 (1), pp. 48–56.
21. D. Chasoglou, E. Hryha, and L. Nyborg: *World PM2010 Proceedings*, Fortezza da Basso Centre, Florence, Italy, 2010, vol. 2, pp. 3–12.
22. E. Hryha and L. Nyborg: *World PM2010 Proceedings*, Fortezza da Basso Centre, Florence, Italy, 2010, vol. 2, pp. 267–74.
23. R.M. German: *Int. J. Powder Metall.*, 1990, vol. 26, pp. 23–34.
24. R.M. German: *Int. J. Powder Metall.*, 1990, vol. 26, pp. 35–43.
25. R.M. German: *Metall. Mater. Trans. A*, 1997, vol. 28A, pp. 1553–67.
26. P.J. Uggowitzer and M. Harzenmoser: *HNS 88*, J. Foct and A. Hendry, eds., The Institute of Metals, London, U.K., 1989, pp. 174–79.
27. F. Vanderschaeve, R. Taillard, and J. Foct: *J. Mater. Sci.*, 1995, vol. 30, pp. 6035–46.
28. N. Krasokha, S. Huth, K. Zumsande, S. Weber and W. Theisen: *World PM2010 Proceedings*, Fortezza da Basso Centre, Florence, Italy, 2010, vol. 2, pp. 259–66.
29. C. Friedrich, G. Berg, E. Broszeit, and C. Berger: *Materialwiss. Werkst.*, 1997, vol. 28, pp. 59–76.
30. A. Sieverts: *Z. Phys. Chem. A*, 1931, vol. 155, pp. 299–313.
31. H. Berns: *Proc. Int. Current Status Seminar on Thermochemical Surface Engineering of Stainless Steel*, 2000, Osaka, Japan, pp. 111–16.
32. F. Schmalt and H. Berns: *Proc. 1st Int. Surface Engineering Congress and the 13th IFHTSE Congress*, 2002, Columbus, OH, pp. 88–97.
33. H. Mitsui and S. Kurihana: *ISIJ Int*, 2007, vol. 47 (3), pp. 479–85.
34. H. Berns: *Materialwiss. Werkst.*, 2002, vol. 33, pp. 5–11.
35. J.D. Fast: *Interactions of Metals and Gases Vol. II, Kinetics and Mechanisms*, Macmillan Press, London, U.K., 1971, pp. 236–42.
36. H.J. Grabke and G. Hörz: *Ann. Rev. Mater. Sci.*, 1977, vol. 7, pp. 155–78.